The Canadian Mineralogist
Vol. 42, pp. 1369-1382 (2004)

VOLUME CHANGES IN FLUID INCLUSIONS PRODUCED BY HEATING AND PRESSURIZATION: AN ASSESSMENT BY FINITE ELEMENT MODELING

PAMELA C. BURNLEY[§] AND M. KATHLEEN DAVIS[¶]

Department of Geology, Georgia State University, Atlanta, Georgia 30303, U.S.A.

ABSTRACT

Recent advances in using the hydrothermal diamond anvil cell (HDAC) to measure homogenization temperatures of inclusions trapped at high pressure have created a need to better understand changes in elastic volume of fluid inclusions experiencing high internal and external pressures. We have used finite element modeling to explore volume changes of fluid inclusions as a function of shape and distance from the free surface at a sample's edge as an aid in understanding their behavior in HDAC studies. We have modeled a variety of oblate and prolate ellipsoids, as well as a disk that has the same cross-section as a negative crystal in quartz and two right cylinders. All of our models have an axisymmetric geometry and assume linear isotropic elasticity. We find that the percent change in volume of an inclusion is primarily a function of the aspect ratio of the inclusion. The presence or absence of corners and the sharpness of internal corners also affect the volume change, but to a lesser extent. Distance to a free surface is only significant for inclusions that are very close to the free surface. This effect is most pronounced for an oblate ellipsoid oriented with its long dimensions parallel to the free surface. For microthermometric studies of fluid inclusions at 1 atm, the changes in elastic volume due to increases in internal pressure are negligible. However, for HDAC studies, where the application of confining pressure allows more extreme conditions to be obtained, changes in elastic volume can be significant, but can be predicted using finite element models.

Keywords: fluid inclusion, finite element modeling, change in elastic volume.

SOMMAIRE

Les progrès récents dus à l'utilisation d'une cellule hydrothermale à enclume de diamant (HDAC) pour mesurer les températures d'homogénéisation d'inclusions piégées à pression élevée requierrent une meilleure compréhension des changements en volume élastique des inclusions fluides subissant des pressions internes et externes élevées. Nous avons utilisé des modèles à éléments finis afin d'explorer les changements en volume élastique des inclusions fluides en fonction de leur forme et de la distance d'une surface libre en bordure d'un échantillon, pour mieux comprendre leur comportement dans les études HDAC. Nous avons adopté comme modèles une variété d'ellipsoïdes aplatis et allongés, de même qu'un disque ayant la même coupe transversale qu'un cristal négatif dans le quartz, et deux cylindres droits. Tous les modèles possèdent une géométrie axisymétrique et supposent une élasticité linéaire isotrope. Le changement en volume d'une inclusion est surtout une fonction du rapport des dimensions de l'inclusion. La présence ou l'absence de coins et l'acuité des coins internes influencent aussi le changement en volume, mais à un degré moindre. La distance séparant l'inclusion d'une surface libre est seulement importante dans le cas d'inclusions qui sont très près de cette surface. Cet effet serait plus prononcé pour un ellipsoïde aplati orienté avec l'axe principal parallèle à cette surface. Pour des applications microthermométriques à des inclusions fluides à un atmosphère, les changements en volume élastique dus à l'augmentation de la pression interne sont négligeables. Par contre, dans le contexte d'études HDAC, où l'application de la pression de confinement permet d'atteindre des conditions plus extrêmes, les changements en volume élastique peuvent être importants, et on peut les prédire en utilisant les modèles à éléments finis.

(Traduit par la Rédaction)

Mots-clés: inclusion fluide, modèles à éléments finis, changements en volume élastique.

§ *E-mail address*: burnley@gsu.edu
¶ *Present address*: Department of Geology, 2534 C.C. Little Building, University of Michigan, Ann Arbor, Michigan 48109-1063, U.S.A.

Introduction

Temperatures of freezing and homogenization determined from fluid inclusions are widely used to estimate pressure and temperature conditions at which fluids were trapped during mineral growth, recrystallization or fracture healing. These estimates rely on the assumption that the fluid inclusions have maintained a constant volume (Roedder 1984). However, some fluid inclusions can generate internal pressures that are high enough to cause the inclusions to decrepitate, leak or stretch before homogenization measurements can be made [see Vityk *et al.* (2000) and references therein]. Until recently, decrepitation and stretching have been significant issues in studies that explore fluid compositions in high-grade metamorphic terranes, or use synthetic inclusions to determine isochores and phase equilibria in systems where the vapor pressure at homogenization is above 200 MPa (Schmidt *et al.* 1998). However, a new technique has been developed (Chou *et al.* 1994, Schmidt *et al.* 1998, Darling & Bassett 2002) that uses a hydrothermal diamond anvil cell (HDAC) (Bassett *et al.* 1993) to apply confining pressure to the inclusions while homogenization measurements are being made, essentially eliminating the problem of decrepitation and stretching. The new technique comes with its own set of challenges, however. When an external confining pressure is applied and higher internal pressures are achieved, elastic changes in volume become significant (Schmidt *et al.* 1998). The measured temperature of homogenization becomes a function of the confining pressure, and the experimentalist must determine which homogenization temperature is the correct one. As one check of internal consistency, investigators have measured the relationship between homogenization temperature and confining pressure and compared it to what would be expected by taking into account volume changes due to the bulk modulus of the quartz host (Darling & Bassett 2002) and the stresses around a spherical inclusion in elastically anisotropic quartz (Schmidt *et al.* 1998). However, the volume change and, in particular, decrepitation behavior are known to be a function of the inclusion shape, size, and distance to the specimen edge (Hall *et al.* 1993, Bodnar *et al.* 1989, Bodnar & Bethke 1984, Pecher 1981, Leroy 1979, Larson *et al.* 1973). We have used finite element modeling to explore the relative importance of shape and proximity to the sample edge in determining elastic changes in volume of fluid inclusions as an aid in understanding fluid-inclusion behavior in diamond-anvil cell studies.

Numerical Models

Numerical models are useful when problems exceed the complexity that can be handled by analytical models. In the case of stresses and strains around expanding or contracting fluid inclusions, it is relatively easy to calculate analytically the behavior of a spherical hole inside a spherical shell of varying dimensions, or a round hole in a plate of varying thickness (*e.g.*, Timoshenko & Goodier 1970, Zhang 1998)**.** Axisymmetric ellipsoids in an infinite medium can also be dealt with analytically (Eshelby 1957, Zimmerman 1991). However, not all fluid inclusions are well approximated by axisymmetric ellipsoids. Many inclusions take on the shape of a negative crystal, are close to the boundaries of the host material, or are otherwise irregular in shape. The deformation behavior of these inclusions can only be effectively modeled using numerical methods. Numerical methods seek to break a problem into discrete components across which an analytical expression can be applied. Two methods that have been used for the analysis of inclusions are boundary-element methods (Whitney *et al.* 2000) and finite element methods (FEM) (*e.g.,* Kenkmann & Dresen 1998, Mancktelow 2002).

Finite element modeling is a method of approximating a solution to differential equations that describe the behavior of a dependent variable over some field by discretizing the problem into elements of a finite size. In the case of stress and strain of a solid body, the body is broken into two- or three-dimensional spatial elements, which form the model mesh. The behavior of the elements is calculated at nodes that occur at the corners and, in some cases, along the edges of the elements. The behavior of each element is coupled to its neighboring elements because elements share the nodes along their common boundaries. The behavior of nodes within an element are dictated by the constitutive equations assigned to that element. These relationships can be expressed as a system of linear equations. Provided that there is a sufficient number of boundary constraints, the solution to the system of linear equations can be obtained by matrix inversion. Typically, the numerical methods used to achieve the matrix inversion are iterative. One's ability to use finite element modeling to calculate a realistic answer is limited by the degree to which the geometry of the model, the material parameters, and the coarseness of the model mesh approximate the modeled object. Another limit is imposed by the amount of CPU time needed to invert the matrix. For two-dimensional models, the size of the matrix to be inverted is equal to the number of nodes in the model squared; for a three-dimensional model, it is equal to the number of nodes cubed. For obvious reasons, two-dimensional models are easier to calculate than three-dimensional models.

There are a number of criteria that one uses to discern whether an FEM model is good. First, the elements must be small with respect to the scale at which one wishes to examine the model. This is because the model uses a linear interpolation between each node or a parabolic fit over three nodes. Therefore, changes in between nodes are not as well known. Areas of less interest can be modeled with larger elements, and computational power thus can be saved to resolve areas with large fluc-

tuations. Second, solutions should be mesh-independent; results from succeeding generations of mesh refinement should converge on a single result, and two different meshes that are both sufficiently refined should yield the same result. Finally, to the maximum extent possible, model results should compare favorably with analytical calculations and experimental observations.

Methods

We have used a commercially available engineering package, MSC MARC/Mentat, to create and analyze 2D axisymmetric finite-element models of fluid inclusions experiencing varying internal (P_I) and external pressures (P_E). All models presented here were constructed using six-noded triangular elements that have a node at each vertex and at the midpoint of each side. The models were calculated assuming a 2D axisymmetric geometry utilizing full integration. We assumed an isotropic linear elastic response for the host material around the inclusion. The constitutive equation used by MARC for linear elastic solids is:

$$\sigma_{ij} = \lambda\Delta_{ij}\varepsilon_{kk} + 2G\varepsilon_{ij} \quad (1)$$

where σ_{ij} is the stress tensor, Δ_{ij} is the Kronecker delta, ε_{ij} is the strain tensor, λ is the Lame constant, and G is the shear modulus. Note that λ can be expressed as

$$\lambda = \nu E/[(1 + \nu)(1 - 2\nu)] \quad (2)$$

and G can be expressed as

$$G = E/[2(1 + \nu)], \quad (3)$$

where ν is the Poisson's ratio and E is the Young's modulus. MARC accepts E and ν as inputs to define a material's elastic properties. For all the models presented here, we used the Young's modulus and Poisson's ratio for polycrystalline quartz (Table 1). The pressure and temperature dependence of the moduli are not included in these calculations. At room temperature, the change in the shear modulus of quartz from 0 to 300 MPa is 0.3%. The bulk modulus increases over the same range by 5.1%. However, in any experiment, this increase will be offset by a decrease in the stiffness due to increasing temperature for example at room pressure, the bulk modulus is 5.5% less at 250°C than at room temperature. Zhang (1998) has shown that for a sphere, the effect of elastic anisotropy is important in making quantitative comparisons with experimental fluid-inclusion data. However, for any shape other than a sphere, the orientation of the shape with respect to the crystallographic axes should also be important. Thus for a quantitative comparison between a particular laboratory measurement and a numerical model, the specific details of inclusion shape, crystallographic orientation and elastic anisotropy will need to be included.

TABLE 1. ELASTIC CONSTANTS FOR POLYCRYSTALLINE QUARTZ

K_s GPa	$\delta K_s/\delta P$	$\delta K/\delta T$ MPa/K	G GPa	$\delta G/\delta P$	$\delta G/\delta T$ MPa/K	E GPa	ν
37.8	6.4	-8.5	44.3	0.46	−0.8	95.6	0.0786

The elastic constants of polycrystalline quartz include the adiabatic bulk modulus K_s, the shear modulus G, and their temperature and pressure derivatives (Bass 1995). Young's modulus E and Poisson's ratio ν used in the finite element models are calculated from the bulk modulus and the shear modulus.

As we wish to use FEM to calculate solutions that cannot be obtained by other means, it is important to know that our method is reliable. We tested a variety of element types to see which ones performed best for our particular problem. All of the element types tested could reproduce the analytical solution for the stress state around a hole in a plate and an empty sphere in a solid to within 2.5% of the peak stress values**.** A six-noded triangular element gave the closest fit, the difference in the peak stress not exceeding 1%. This element (element 126 in the MARC library) uses a parabolic interpolation function along each edge.

An iterative process was used to develop each model mesh. The first mesh for a given inclusion was built to capture the basic geometry, with the smallest elements near the inclusion and the largest elements furthest away. Material properties and boundary conditions were assigned, and then the meshes were analyzed using MARC. The location of stress concentrations and gradients in stresses were noted; the mesh in these areas was then refined until the stress contours appeared smooth. In addition, the models were checked for any deflections of the outer edges caused by the presence of the inclusion at the center of the model. If changes in displacement along the outer edges of a model were greater than 10^{-6} of the model dimensions, more material was added to the exterior of the model. Element sizes in the final models vary over two to three orders of magnitude, and the outer dimensions of the full models are about 20 times the long dimensions of the inclusion. Models used to study the effect of the proximity of the sample edge to the inclusion were made by truncating full models. Two meshes are shown as examples in Figure 1.

Boundary Conditions

All axisymmetric models have their axis of rotational symmetry along the horizontal axis (x axis). Therefore, a boundary condition of no translation in the vertical direction (y axis) was applied to all nodes that lay on the x axis. For models that had a mirror plane perpendicular to the axis of rotational symmetry, half the shape was modeled and a boundary condition specifying no translation in the direction of the x axis was applied to nodes lying on the mirror plane. Pressure is modeled by

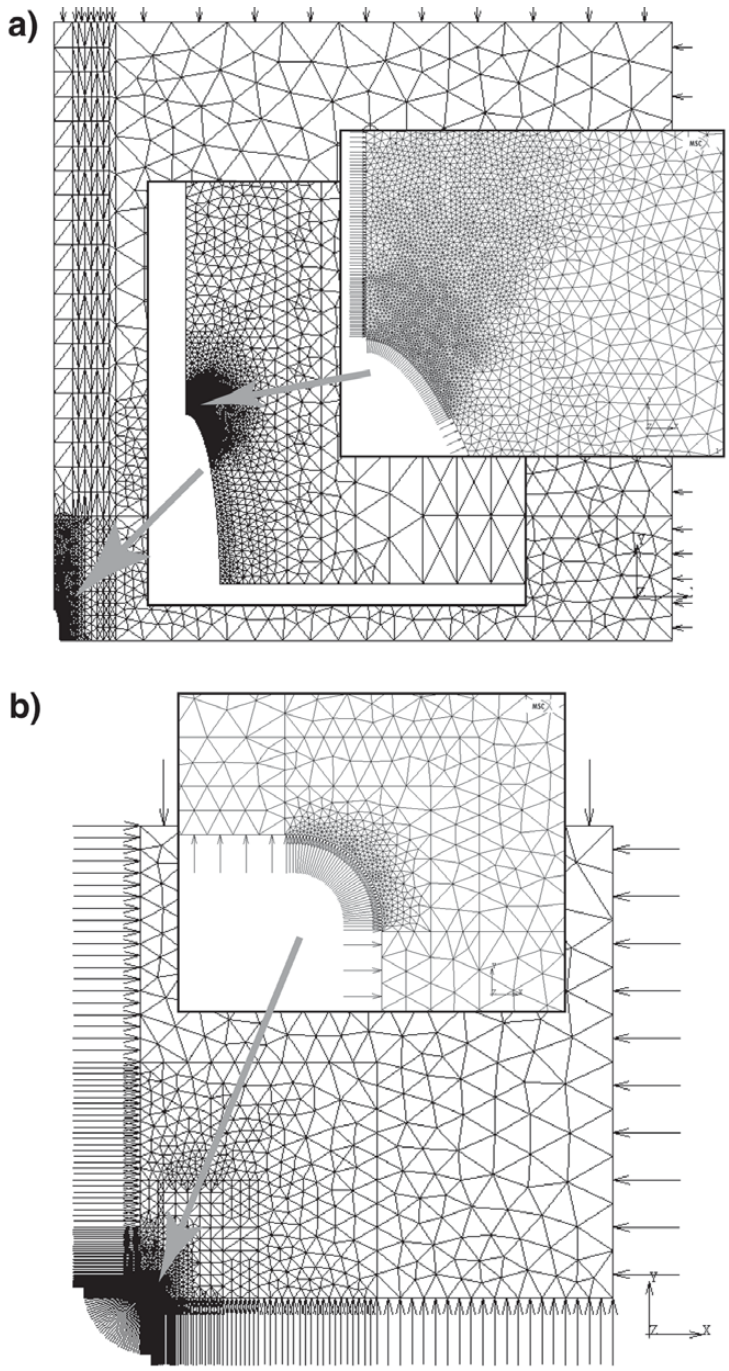

FIG. 1. Two examples of finite-element meshes used in modeling. Each triangular element has six nodes, one at each vertex and one at the center point of each side. The nodes are not plotted here so that the details of the mesh can be seen. Arrows pointing at nodes and edges indicate boundary conditions applied at those locations. A) This model was used for the oblate ellipsoid with a 1:5 aspect ratio. The model is constructed so that the right-hand side can be removed in steps in order to study the effect of distance to the free surface. The insets show progressive levels of detail of the mesh near the inclusion. B) This model was used for the right cylinder with a radiused internal corner (right cylinder II). The inset shows the meshing at the radiused corner.

the application of constant edge-loads to the external boundaries of the models. Edge loads in MARC are assumed to have the same units as the elastic moduli (*e.g.*, GPa) and are distributed along the edge of the element, which for an axisymmetric model represents an area. MARC uses numerical integration to calculate equivalent nodal loads given the dimensions of the area over which the distributed load is applied. To simulate the confining pressure, constant edge-loads were applied on the external boundaries of the model. Another set of edge loads was applied to the internal boundary of the inclusion to simulate the pressure generated by the fluid (for examples, see Fig. 1).

Model Shapes

We have modeled a variety of oblate and prolate ellipsoids, a pointed disk, and two right cylinders, one with perfectly sharp internal corners (right cylinder I) and one with radiused internal corners (right cylinder II). The pointed disk, which we refer to as the "disk with three corners", is shown in Figure 2. To build this model, we used a profile derived from a photomicrograph of a natural H_2O–NaCl–CO_2-bearing inclusion in quartz (Blount *et al.* 1999, Davis & Burnley 2000) from a vein in Piedmont basement rocks beneath the Savannah River DOE site in Savannah, Georgia (La Tour *et al.* 1995). At the level of resolution of the optical microscope, the internal corners of the inclusion appear to be sharp; however, rounding of the corners at some scale is to be expected. The refinement of the mesh around the stress concentrations generated at corners requires the model mesh to contain details at a much finer scale than can be resolved optically. Therefore, in order to determine the degree to which the internal corners should be rounded, we used transmission electron microscopy (TEM). A chip of the same quartz vein that contained the inclusion that we used for the model was thinned using an Argon ion mill with a liquid nitrogen cooled stage. The sample was imaged at 200 kV using a JEOL 2010 TEM located at MVA Inc. in Norcross, Georgia. The radius of curvature for the internal corners for several inclusions was measured and compared with the longest dimension of the inclusion visible in the TEM foil (Fig. 3). We found that for this particular specimen, the radius of curvature ranged from 0.05 to 0.5 μm or 1–15% of the inclusion's long dimension. The relative measurement is useful for comparison with the models, which

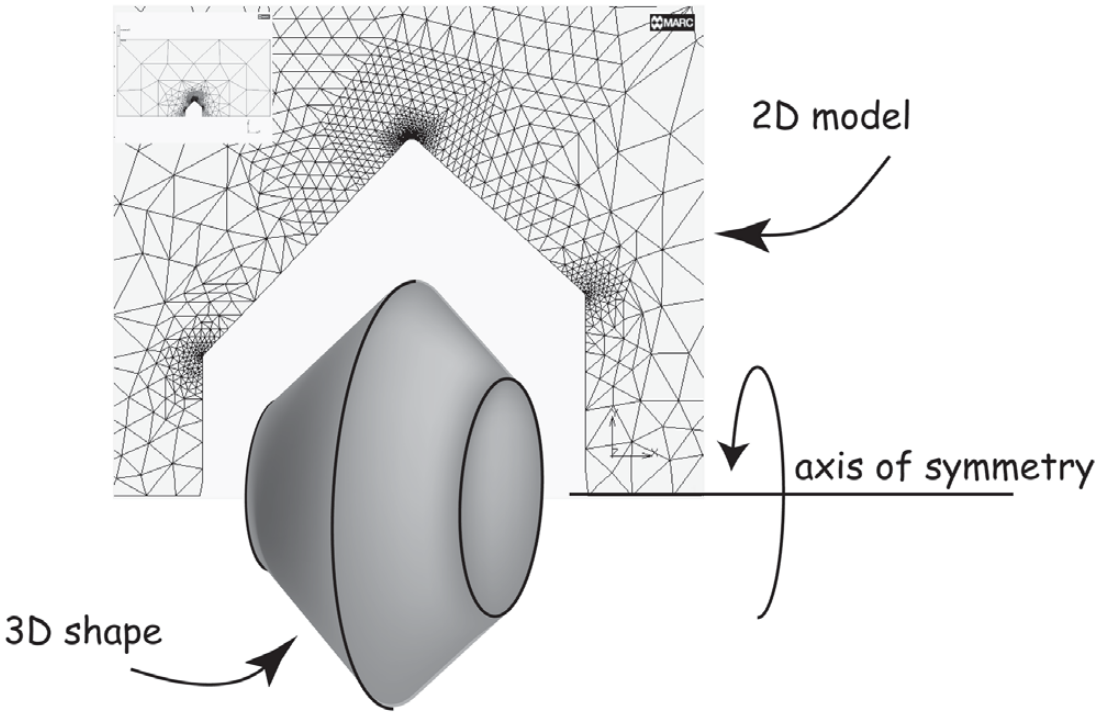

FIG. 2. The diagram shows the model mesh for the disk with three corners. The model is spun about the *x* axis to create a 3D volume of revolution. The inset shows the entire mesh. The mesh was drawn from a profile of a natural inclusion in quartz.

are dimensionless. For the disk with three corners, the corners were meshed with a radius of curvature ranging from 1 to 10% of the model's long dimension. Right cylinder I was meshed with a sharp 90° corner, and right cylinder II built with an internal corner with a radius of curvature of 5% of the model's edge-length (Fig. 1b).

Ultimately, we wish to check the predictions of models against the behavior of real fluid inclusions. In such a study, the many assumptions that go into the models, including inclusion shape, isotropic elasticity, and the level of detail captured by the mesh, can also be examined.

Volume Calculations

MARC output includes the undeformed node positions and their change in position. The deformed and undeformed volume of the inclusions was calculated by numerical integration. For shapes that can be described analytically, the undeformed volume calculated from each model fits the volume obtained by integration to within 0.1%. Planes were fit to the percent change in volume as a function of P_I and P_E. Owing to the iterative nature of the modeling process, errors in stress and nodal displacement are expected to be about 2%.

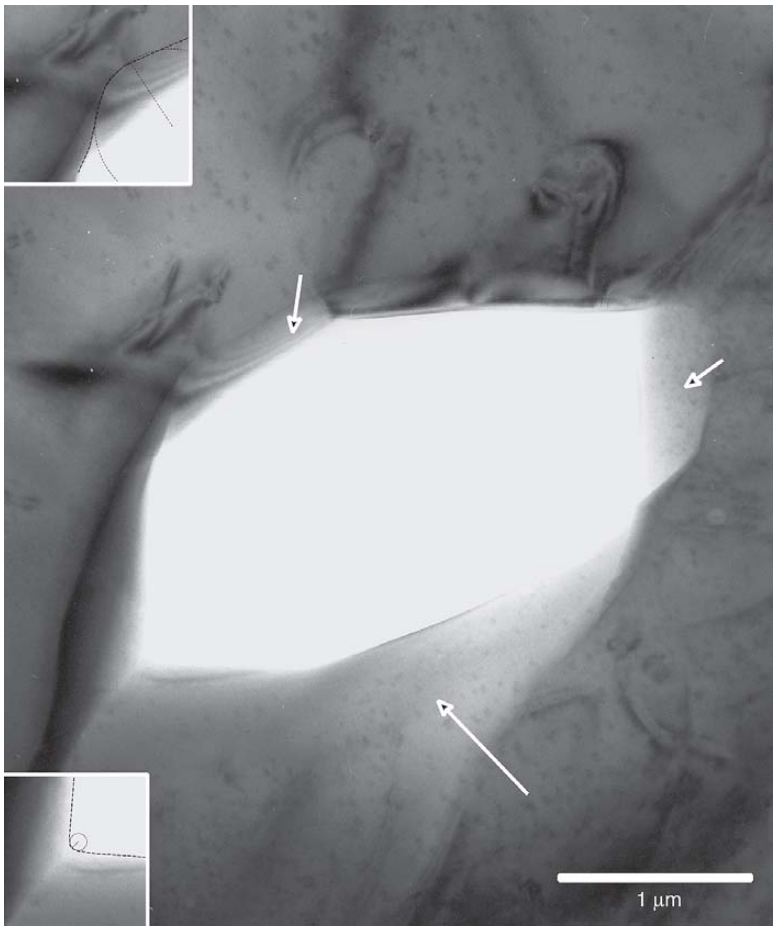

FIG. 3. TEM micrograph of a fluid inclusion in quartz from the Piedmond basement at the Savannah River site. The inclusion cuts through the foil at an angle, giving rise to extra thin regions around the edge of the inclusion (arrows). Insets at the top and bottom show tracings of the corner geometry as well as the radius of curvature. Accelerating voltage was 200 kV. Scale bar is 1 μm.

Depiction of Results

Each model can be described as a plane in a parameter space defined by volume change, internal pressure (P_I), and external pressure (P_E) (Fig. 4). Since what is important about the spatial dimension of each model is the relative dimension, the volume change can be depicted in terms of percent change in volume relative to the volume of the original model (V_c).

$$V_c = (V_{\text{deformed}} - V_{\text{undeformed}})/V_{\text{undeformed}} \times 100 \quad (4)$$

All models should intersect the origin of this coordinate space and share a line in the plane $P_E = P_I$, along which the volume change is dictated by the bulk modulus alone, as no shear stresses are generated in the absence of differential pressure. It is useful to depict the models by taking vertical sections through this space (as shown in Figs. 5 and 6). Because all models share this common line in the plane where $P_E = P_I$, the difference in volume change between any two models (ΔV_c) is a linear function of the differential pressure (ΔP), where:

$$\Delta P = P_I - P_E \quad (5)$$

which can be written as:

$$\Delta V_c = m\Delta P \quad (6)$$

An example of this approach can be seen later (in Fig. 11). The difference in percent change in volume between any two models can be characterized by the slope (m) of this line; the larger the value of m, the greater the difference between the behavior of the models. This method of collapsing the difference between two models to a single point is used in Figure 7.

Results

Effect of shape

Curves describing the volume change in "quartz" as a host (recall that by this we mean an isotropic material with the same elastic moduli as polycrystalline quartz) as a function of internal pressure for eight shapes are

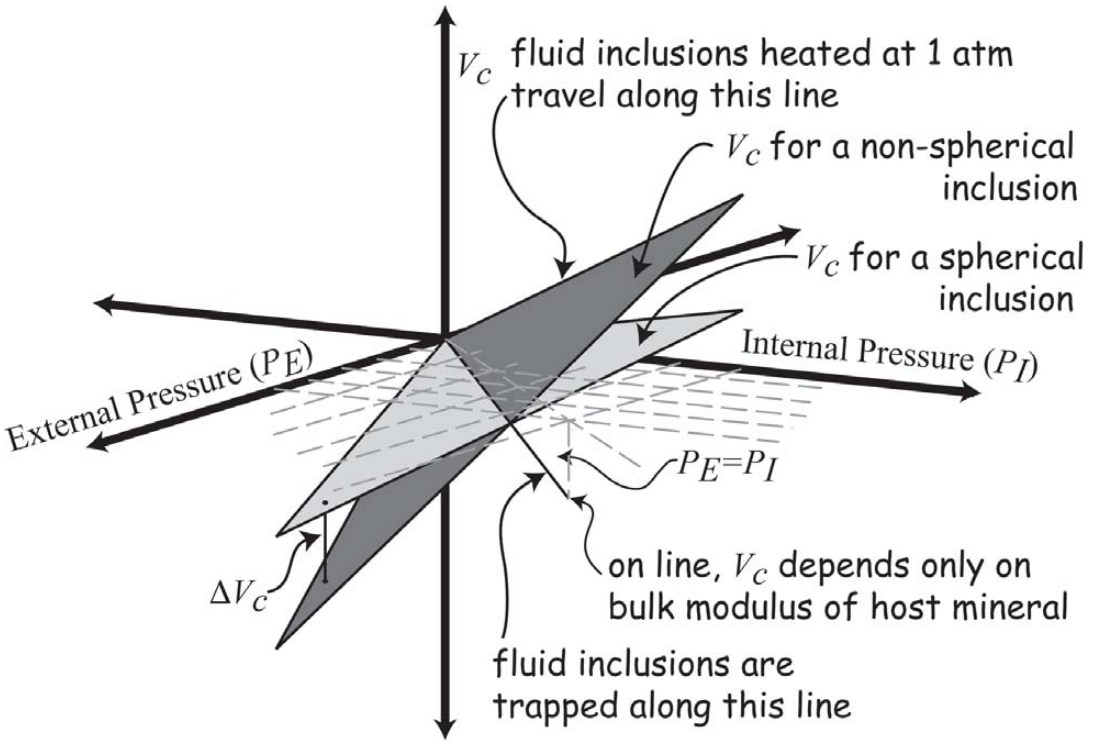

FIG. 4. Diagram of the parameter space used in this study. Planes represent the behavior of fluid inclusions in the parameter space. Because all of the models share a line in the plane $P_I = P_E$, which is dictated by the bulk modulus, the difference in V_c between any two models is a linear function of ΔP. The larger the slope (m) of this line, the greater the difference in volume change between the two inclusions.

shown in Figure 5. Coefficients for the equation describing the percent change in volume (V_c) as a function of P_I and P_E are presented in Table 2. The 2:1 prolate and oblate ellipsoids have been meshed twice, and coefficients for V_c are reproducible to within <1%. As expected, all of the inclusions experience the same change in volume if P_I is equal to P_E. Under this condition, there is no differential stress in the material around the inclusion, and the bulk modulus alone governs the volume change. The average V_c of the models along the line where $P_I = P_E$ differs from that predicted by theory by 0.4%, and the models vary no more than 0.2% from each other. Figure 6 shows V_c as a function of P_E for eight inclusion shapes plotted for a constant internal pressure of 200 MPa. Notice that the models all intersect at 200 MPa where $P_I = P_E$. Inclusions that expand the most when the internal pressure is greatest also collapse more readily when the external pressure is greatest.

Effect of sample edges

Proximity to the sample edge will also have an impact on volume change if the sample edge is close enough to the inclusion. We examined two cases: 1) inclusions that are centered in a plate of varying thickness, and 2) inclusions that are close to one edge of a very thick plate. For each shape, the axis of rotational symmetry is normal to the free surface. In order to display the effect of proximity to the edge, the strategy of characterizing the difference between two models as a single point, as discussed above, was used. The difference between the volume change experienced by an inclusion located at a very large distance from any external boundary and the same inclusion sitting in the center of a thin plate is divided by ΔP and plotted in Figure 7. To compare different shapes, the thickness of the wall between the inclusion and the free surface is divided by

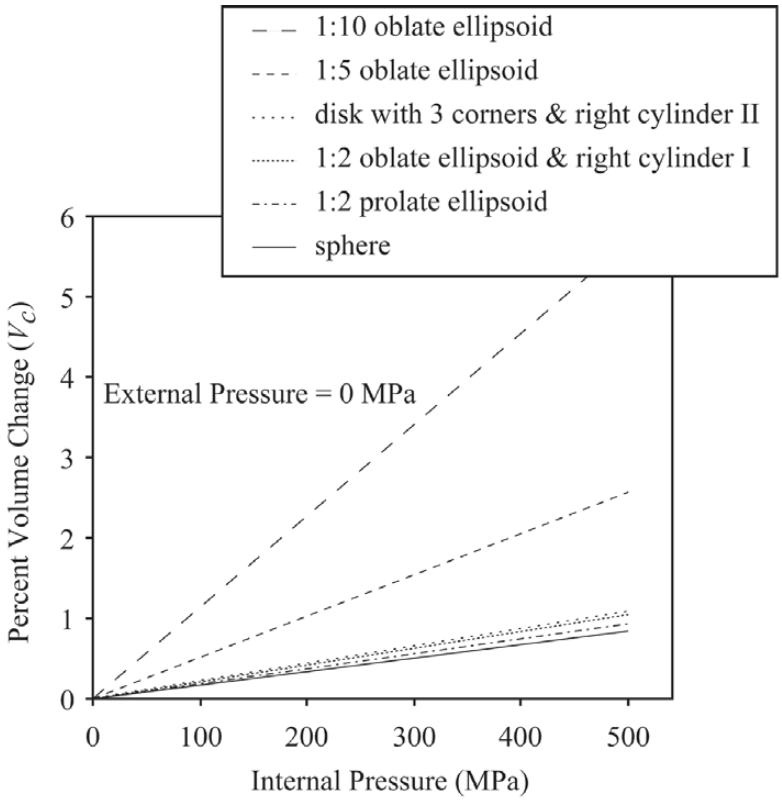

FIG. 5. Percent change in volume (V_c) as a function of internal pressure (P_I) when external pressure is 0 MPa for an inclusion shaped like a sphere, three oblate ellipsoids with different aspect ratios, a prolate ellipsoid, two right cylinders and a disk with three corners.

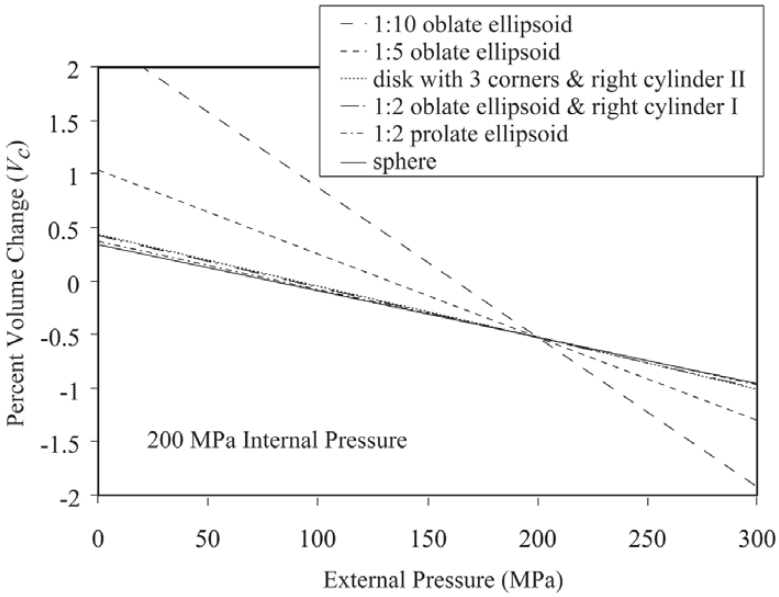

FIG. 6. Percent change in volume as a function of external pressure (P_E) for an inclusion shaped like a sphere, several oblate ellipsoids with different aspect ratios, a prolate ellipsoid, two right cylinders and a disk with three corners, all with an internal pressure of 200 MPa. The lines intersect where the internal and external pressures are equal because the differential stress within the matrix is zero at that point.

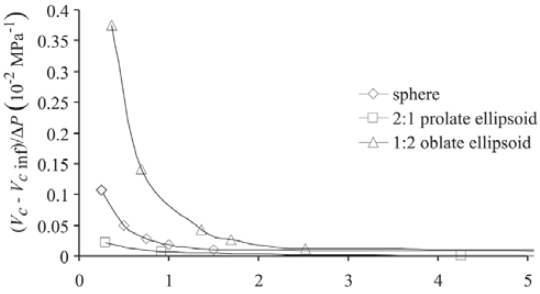

FIG. 7. A plot showing the effect of distance from the free surface on changes in elastic volume for a sphere, 2:1 prolate ellipsoid and a 1:2 oblate ellipsoid. Each point on the plot represents the behavior of an inclusion in a thin plate compared to the same inclusion in a very thick plate. The difference between any two models is a linear function of ΔP; $\Delta V_c = m\Delta P$. The slope m, a measure of the degree of difference, is plotted on the y axis. The x axis gives the thickness of the host between the inclusion edge and the sample surface divided by the radius of a sphere that has the same volume as the inclusion. This approach allows a comparison of different models.

TABLE 2. COEFFICIENTS USED IN CALCULATING PERCENT INCREASE IN VOLUME AS A FUNCTION OF INTERNAL AND EXTERNAL PRESSURE FOR VARIOUS SHAPES OF FLUID INCLUSION

	a	b
Oblate ellipsoid (10:1)	0.0114	-0.0140
Oblate ellipsoid (1:5)	0.00515	-0.00778
Right cylinder I	0.00220	-0.00484
Disk with three corners	0.00219	-0.00482
Oblate ellipsoid (1:2)	0.00210	-0.00474
Right cylinder II	0.00210	-0.00473
Prolate ellipsoid (1:2)	0.00185	-0.00448
Sphere	0.00169	-0.00432

The increase in volume is given by $V_c = a P_i + b P_e$. The external boundaries for these models are located very far from the inclusion.

the radius of a sphere that has the same volume as the inclusion; this value is plotted along the x axis. Results for three shapes (a sphere, a 1:2 oblate ellipsoid and a 2:1 prolate ellipsoid) are shown in Figure 7, and the model geometry for the 2:1 prolate ellipsoid and the sphere are shown in Figure 8. For an inclusion sitting close to one edge of a thick plate, the geometry relevant to a fluid-inclusion study, we find that V_c can be approximated (to within 5%) by averaging the volume change for a symmetric thin-walled and a thick-walled model.

Discussion

Elastic changes in volume are clearly a function of shape, and the most important characteristic of an inclusion's shape appears to be its aspect ratio. The effect of corners is less important. Both the disc with three corners and the 1:2 oblate ellipsoid have the same aspect ratio, but the disk with three corners experiences only slightly larger changes in volume. The effect of the sharpness of the corners also is quite small. The coefficients for the equation describing the V_c for right cylinder I (sharp internal corners) and right cylinder II (radiused internal corners) differ by only 5% (Table 2). Whitney *et al.* (2000) found similar results in their boundary-element study of fractures around solid inclusions: aspect ratio was found to be the most important characteristic in predicting fracture patterns. Zimmerman (1991) has shown that corner sharpness also has little effect on the volume change of infinite channels that have a four-sided hypotrochoidal cross-section. By far the largest changes in volume seen amongst the shapes modeled are in the oblate ellipsoid models. Although the more equant shapes display only minor changes in volume at low internal pressure, the high-aspect-ratio oblate ellipsoids experience elastic changes in volume that could be important (depending on the equation of state of the fluid) for measurements of temperature of homogenization. However, it is important to keep in mind that the differential stress along the internal surfaces of these shapes can become extremely high as well. For example, the quartz at the end of the 1:5 oblate ellipsoid will experience >500 MPa differential stress when under an internal overpressure of 100 MPa (Fig. 9). Therefore, these inclusions would also be more likely to stretch or fracture at room pressure. These model results emphasize the importance of using caution when working with inclusions with plate or crack-like shapes.

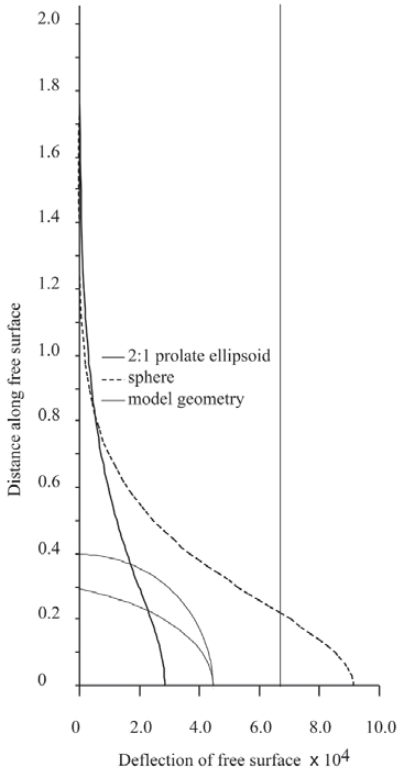

FIG. 8. Plot comparing the edge deflection of a spherical inclusion and a 2:1 prolate ellipsoid in a thin plate. The *x* axis gives the deflection. The geometry is drawn to the same scale as plotted on the *y* axis; the model extends a distance of 18 units beyond the top of the plot. The vertical line shows the position of the free surface relative to the inclusions. The deflections are plotted for $P_I - P_E = 200$ MPa. The 2:1 prolate ellipsoid deforms the surface significantly less, and therefore its volume change relative to that in a very thick host is less sensitive to the distance to the free surface.

From Figure 7, we can see that inclusions must be relatively close to the sample edge before there is any appreciable change in V_c. The additional change in volume is caused by the stresses surrounding the inclusion encountering and causing a deflection of the model edge. To first order, these stresses fall off with distance cubed (Eshelby 1957), as seen in Figure 9, which is why the effect is only seen where the wall is relatively thin (Fig. 7). Since the shape of the stress field around the inclusion is a function of the inclusion's shape, the importance of proximity to the sample edge will also be a function of shape. A non-intuitive observation is that the effect is less pronounced for the 2:1 prolate ellipsoid than for the sphere, even though the 2:1 prolate ellipsoid has a larger peak stress in the wall between it and the free surface (166 MPa *versus* 133 MPa for $\Delta P =$ 100 MPa). However, because the sphere does not fall away from the free surface at the same rate as the 2:1 prolate ellipsoid, the sphere creates larger stresses over a greater area of the free surface, which deforms more (Fig. 8). This relationship remains true even if one compares a 2:1 prolate ellipsoid with a sphere whose radius is the same as the minor axis of the 2:1 prolate ellipsoid. The largest effect is seen for the 1:2 oblate ellipsoid, which has the largest relative proportion of its surface area close to the free surface. Using Figure 7, we predict that an elliptical inclusion 40 μm across and 20 μm thick centered in a plate 32 μm thick, experiencing a 100 MPa overpressure, would have an additional 0.38% volume change beyond what would be expected for the same inclusion in an infinite host. The same inclusion 6 μm below the surface of a thick plate would experience about 0.19% additional increase in volume.

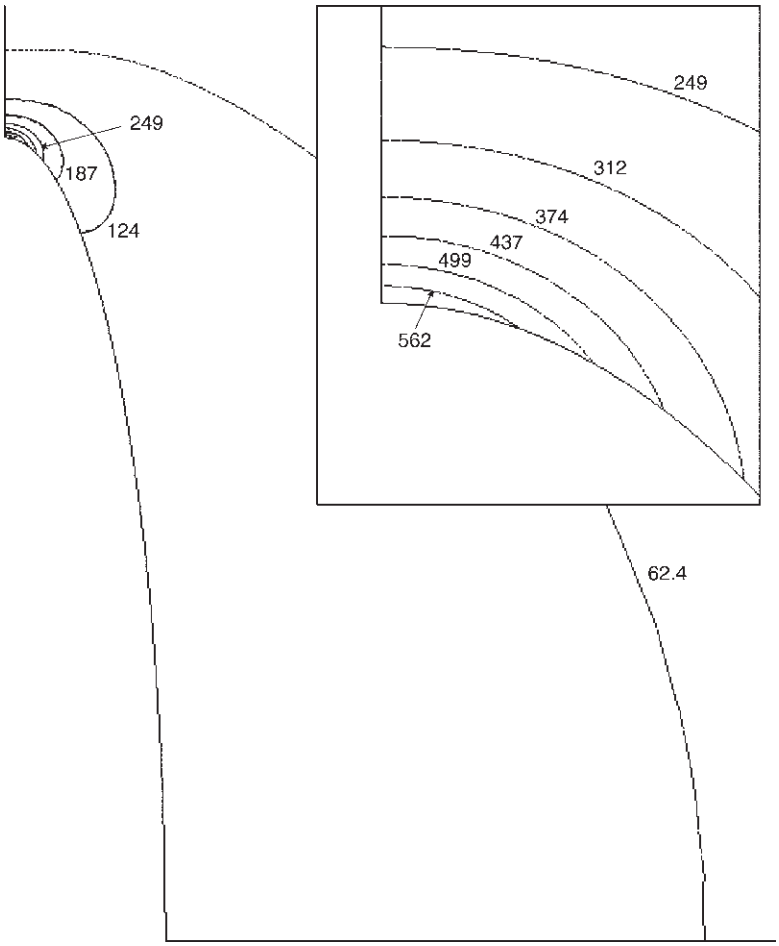

FIG. 9. Plot of contours for constant differential stress in the quartz host around a 1:5 oblate ellipsoidal inclusion experiencing 100 MPa internal pressure and 0 MPa external pressure. The outer boundaries of the quartz host are at a distance of 20 times the long dimension of the inclusion. Numbers plotted beside the contours represent differential stress in MPa.

Application

For most fluid-inclusion work, volume changes due to elastic deformation are negligible, even for the 1:10 oblate ellipsoid, the most extreme shape tested. For example, for fluid inclusions containing H_2O, pressures at homogenization cannot exceed 220.55 bars (Haar *et al.* 1984). Such a pressure yields changes in homogenization temperature that are at most 0.3°C (Fig. 10), which would not be observable in a typical heating experiment. However, for inclusions containing several components, internal pressures at homogenization can become quite large. For example, CO_2–H_2O liquids can show immisciblity at pressures well over 2 GPa [see Diamond (1994) for review]. These homogenization temperatures cannot be measured without the application of confining pressure because the inclusions will decrepitate (Schmidt *et al.* 1998, Darling & Bassett 2002). It is in hydrothermal diamond-anvil cell studies, where the difference between internal and external pressure of the inclusion can reach 100 MPa or more, that these calculations are most useful. In the system CO_2–H_2O–NaCl, small changes in molar volume can lead to measurable changes in homogenization temperature (Schmidt *et al.* 1998). For example, Darling & Bassett (2002) calculated that a 0.22% change in molar volume should cause

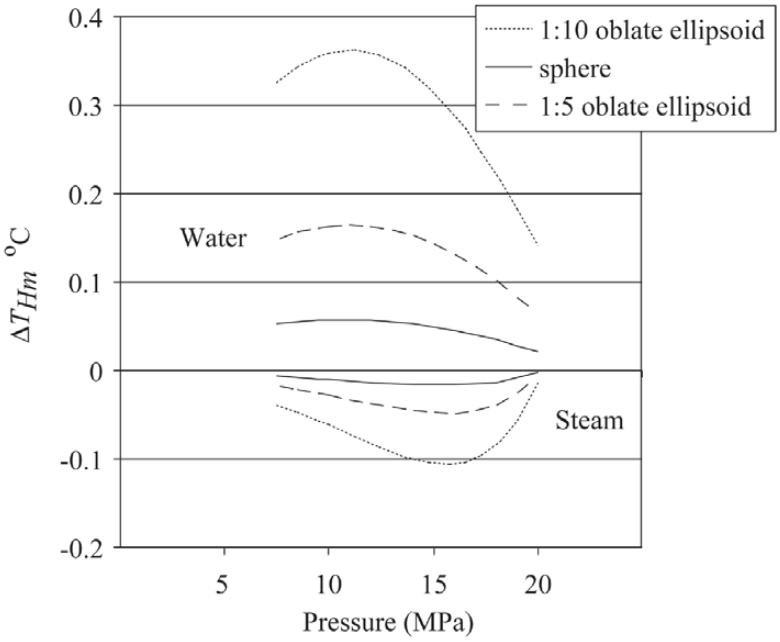

FIG. 10. Change in temperature of inclusion homogenization ΔT_{Hm} due to changes in elastic volume as a function of pressure for pure H_2O. For inclusions homogenizing to liquid water, the shift in homogenization temperature is positive. For inclusions homogenizing to steam, the shift in homogenization temperature is negative.

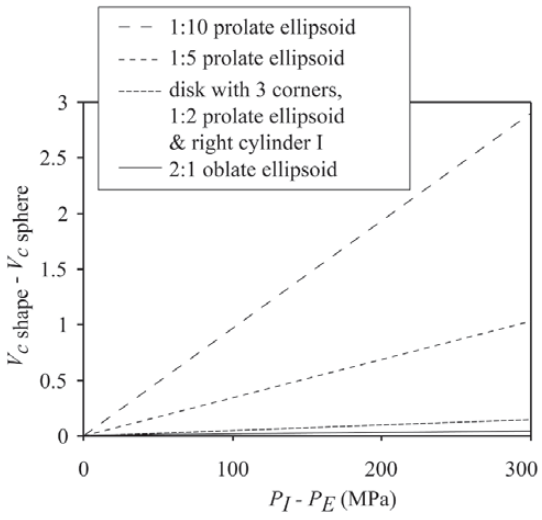

FIG. 11. Difference between percent change in volume for a spherical inclusion and inclusions of other shapes (ΔV_c) as a function of the difference between the external and internal pressure (ΔP). This difference is a measure of the error produced by assuming that an inclusion is spherical. For the more equant shapes tested, this assumption is good. For oblate ellipsoids with higher aspect-ratios, measurable deviations in homogenization temperature may occur.

a 2.8°C change in the temperature of total homogenization of natural CO_2–H_2O–NaCl inclusions in their study.

It is relatively straightforward to calculate the volume change of a sphere using analytical methods (Zhang 1998). Therefore, it is important to know how much error is produced by assuming that an inclusion is a sphere if the shape is in fact not a sphere. In Figure 11, we plot the difference between the volume change of a sphere and the other inclusion shapes as a function of ΔP. As discussed before, if ΔP is zero, the volume change is a function only of the bulk modulus of quartz, and inclusion shape is not a factor. From Figure 11, it can be seen that only the oblate shapes with high aspect-ratios are likely to cause significant deviations from what is predicted by using a spherical model.

CONCLUSIONS

The results of this analysis confirm what studies of fluid inclusions at room pressure have already shown empirically: elastic changes in volume in a quartz host at internal overpressures, insufficient to cause the decrepitation, are not important to measurements of homogenization temperature. However, if inclusions are studied at high external pressure, significant differential pressures can be achieved, and elastic changes in volume can significantly affect measured temperatures

of homogenization. At least for the axisymmetric shapes studied here, these volume changes are primarily a function of the inclusion's aspect ratio. Details of the shape, such as the presence and sharpness of internal corners, and the proximity of the inclusion to a free surface, also have an effect, but these are secondary to the effect of aspect ratio.

Acknowledgements

This work was supported by National Science Foundation grant EAR–9706289 and its REU supplement as well as by EAR–9820666 and EAR–0136107. The authors thank MVA Inc. of Norcross, Georgia for the use of their TEM and MVA's microscopist, Lindsay Keller, for assistance with the TEM. We thank David Vanko, Aditya Kar, Bob Bodnar and Leonid Germanovich for advice on fluid inclusions and numerical modeling, Bill Bassett for pointing out the need for this study, and Martin Dunn for assistance with FEM and MARC in particular. Drs. R. Bakker and Y. Zhang provided careful and helpful reviews.

References

Bass, J.D. (1995): Elasticity of minerals, glasses and melts. *In* Mineral Physics and Crystallography: a Handbook of Physical Constants (T.J. Ahrens, ed.). The American Geophysical Union, Washington, D.C.

Bassett, W.A., Shen, A.H., Bucknam, M. & Chou, I-Ming (1993): A new diamond anvil cell for hydrothermal studies to 2.5 GPa and from –190 to 1200°C. *Rev. Sci. Instrum.* **64**, 2340-2345.

Blount, M., Kar, A., Dozier, C. & Vanko, D.A. (1999): A study of natural H_2O–CO_2–NaCl fluid inclusions from metamorphic quartz in a basement sample from the Savannah River site, South Carolina. *Geol. Soc. Am., Southeastern Sect., Abstr. Programs* **32**, A6.

Bodnar, R.J. & Bethke, P.M. (1984): Systematics of stretching of fluid inclusions. I. Fluorite and sphalerite at 1 atmosphere confining pressure. *Econ. Geol.* **79**, 141-161.

_____, Binns, P.R. & Hall, D.L. (1989): Synthetic fluid inclusions. VI. Quantitative evaluation of the decrepitation behavior of fluid inclusions in quartz at one atmosphere confining pressure. *J. Metamorph. Geol*. **7**, 229-242.

Chou, I-Ming, Shen, A.H. & Bassett, W.A. (1994): Application of the hydrothermal diamond-anvil cell in fluid inclusion research. *In* Fluid Inclusions in Minerals, Methods and Applications (B. De Vivo & M.L. Frezzotti, eds.). *Short Course of the IMA Working Group, Inclusions in Minerals* (*Pontignano*). Virginia Tech, Blacksburg, Virginia (215-230).

Darling, R.S. & Bassett, W.A. (2002): Analysis of natural H_2O + CO_2 + NaCl fluid inclusions in the hydrothermal diamond anvil cell. *Am. Mineral.* **87**, 69-78.

Davis, M.K. & Burnley, P.C. (2000): Finite element modeling of stresses developed around fluid inclusions in quartz. *Trans. Am. Geophys. Union* (*Eos*) **81**(19), S39 (abstr.).

Diamond, L.W. (1994): Introduction to phase relations of CO_2–H_2O fluid inclusions. *In* Fluid Inclusions in Minerals: Methods and Applications (B. De Vivo & M.L. Frezzotti, eds.). *Short Course of the IMA Working Group, Inclusions in Minerals* (*Pontignano*). Virginia Tech., Blacksburg, Virginia (131-158).

Eshelby, J.D. (1957): The determination of the elastic field of an ellipsoidal inclusion, and related problems. *Proc. R. Soc. London* **241**, 376-396.

Haar. L.H., Gallagher, J.S. & Kell, G.S. (1984) NBS/NRC *Steam Tables: Thermodynamic and Transport Properties and Computer Programs for Vapor and Liquid States of Water in SI Units.* Hemisphere Publishing Corporation, Washington, D.C.

Hall, D.L., Sterner, S.M. & Wheeler, J.R. (1993): One-atmosphere decrepitation behavior of synthetic fluid inclusions in natural calcite: implications for preservation of calcite-hosted inclusions during burial. *ECROFI XII Abstr., Archiwum Mineralogiczne* **49**, 91-92.

Kenkmann, T. & Dresen, G. (1998): Stress gradients around porphyroclasts: palaeopiezometric estimates and numerical modelling. *J. Struct. Geol.* **20**, 163-173.

Larson, L.T., Miller, J.D., Nadeau, J.E. & Roedder, E. (1973): Two sources of error in low temperature inclusion homogenization determination, and corrections in published temperatures for the East Tennessee and Laisvall deposits. *Econ. Geol.* **68**, 113-116.

La Tour, T.E., Roden, M.F., Vanko, D.A. & Whitney, J.A. (1995): Crystalline basement core – Savannah River site. *Final Report*, *ERDA Task* **53**.

Leroy, J. (1979): Contribution à l'étalonnage de la pression interne des inclusions fluides lors de leur décrépitation. *Bull. Minéral.* **102**, 584-593.

Manckтelow, N.S. (2002): Finite-element modelling of shear zone development in viscoelastic materials and its implications for localisation of partial melting. *J. Struct. Geol.* **24,** 1045-1053.

Pecher, A. (1981): Experimental decrepitation and re-equilibration of fluid inclusions in synthetic quartz. *Tectonophysics* **78**, 567-583.

Roedder, E. (1984): Fluid Inclusions. *Rev. Mineral.* **12**.

Schmidt, C., Chou, I-Ming, Bodnar, R.J. & Bassett, W.A. (1998): Microthermometric analysis of synthetic fluid inclusions in the hydrothermal diamond-anvil cell. *Am. Mineral.* **83**, 995-1007.

Timoshenko, S.P. & Goodier, J.N. (1970): *Theory of Elasticity*. McGraw-Hill, New York, N.Y.

VITYK, M.O., BODNAR, R.J. & DOUKHAN, J.-C. (2000): Synthetic fluid inclusions. XV. TEM investigation of plastic flow associated with reequilibration of fluid inclusions in natural quartz. *Contrib. Mineral Petrol.* **139**, 285-297.

WHITNEY, D.L., COOKE, M.L. & DUFRANE, S.A. (2000): Modeling of radial microcracks at corners of inclusion in garnet using fracture mechanics. *J. Geophys. Res.* **105B**, 2843-2853.

ZHANG, YOUXUE (1998): Mechanical and phase equilibrium in inclusion–host systems. *Earth Planet. Sci. Lett.* **157**, 209-222.

ZIMMERMAN, R.W. (1991): *Compressibility of Sandstone*. Elsevier, Amsterdam, The Netherlands.

Received November 3, 2002, revised manuscript accepted March 6, 2004.